Tetrahedron 75 (2019) 130459

Contents lists available at ScienceDirect

Tetrahedron

journal homepage: www.elsevier.com/locate/tet

Novel dibenzothiophene chromophores with peripheral barbituric acceptors

Michaela Sperátová [a], Jaroslaw Jedyrka [b], Oldřich Pytela [a], Iwan V. Kityk [b], Ali H. Reshak [c, d], Filip Bureš [a], Milan Klikar [a, *]

[a] Institute of Organic Chemistry and Technology, Faculty of Chemical Technology, University of Pardubice, Studentská 573, Pardubice, 53210, Czech Republic
[b] Faculty of Electrical Engineering, Institute of Electronic Systems, Czestochowa University of Technology, Armii Krajowej 17, Czestochowa, 42-201, Poland
[c] Nanotechnology and Catalysis Research Center (NANOCAT), University of Malaya, Kuala Lumpur 50603, Malaysia
[d] Physics Department, College of Science, Basrah University, Basrah, Iraq

ARTICLE INFO

Article history:
Received 24 May 2019
Received in revised form
27 June 2019
Accepted 10 July 2019
Available online 13 July 2019

Keywords:
Dibenzo[*b*,*d*]thiophene
N,*N*′-Dibutylbarbituric acid
Chromophore
π-Conjugated system
Knoevenagel condensation

ABSTRACT

A series of novel chromophores based on central 2,8-disubstituted dibenzothiophene (DBT) or dibenzothiophene-*S*,*S*-dioxide (DBTO) has been designed and prepared. The interconnection of DBT(O) central scaffold with two peripheral barbituric acceptors via various π-spacer allowed significant property tuning of target chromophores. Four new final chromophores and six DBT(O)-intermediates have been successfully synthesized and fully characterized. Experimental and calculated data showed that the fundamental properties are affected by the chromophore A-π-D-π-A or A-π-A-π-A arrangement (DBT vs. DBTO) and the π-linker (ethenylene vs. ethynylene). Thorough structure-property relationships have been elucidated and discussed in detail.

1. Introduction

Organic π-conjugated systems equipped with electron donating and withdrawing substituents, so-called push-pull D-π-A chromophores, found manifold applications in the field of material chemistry [1–5]. Among ordinary electron donors featuring positive mesomeric effect such as NR_2 or OR groups, thiophene occupies a prominent position due to its donating power, planarity, and high polarizability [6]. Thiophene can also be fused with another (hetero)aromatic rings to improve and modify its electronic properties. Thieno[3,2-*b*]thiophene (TT) [7] or dibenzo[*b*,*d*]thiophene (DBT) [8] are two typical representatives. DBT is a popular central building block used for the construction of various π-conjugated molecules, which found application in modern optoelectronics. The popularity of the DBT is not only due to its electronic features but also its facile and selective halogenation and further modification via cross-coupling reactions. For instance, bromination of the DBT using Br_2 is selective to the positions 2 and 8 [9]. Moreover, the sulfur atom undergoes easy oxidation by H_2O_2 to DBT-*S*,*S*-dioxide (DBTO) [10], which leads to a singular switching of the electronic properties (donor→acceptor). Subsequent bromination of DBTO provides 3,7-disubstituted derivative which completes the portfolio of easily accessible DBT(O) isomeric chromophores [11]. Based on these parent DBT(O) scaffolds, mostly symmetrical chromophores were assembled upon introducing *D*, *A* or π moieties. DBT(O) core is very often decorated by polycyclic aromatics such as fluorene [12], fluoranthene [13], anthracene [14], etc. These extended π-systems guarantee remarkable fluoresce. Emissive properties were also encountered for *D*-π-DBT(O)-π-*D* systems with triphenylamine [15–17], acridine [18], carbazole [19–21], or thiophene [22] peripheral donors. Opposite arrangement with peripheral acceptors (*A*-π-DBT(O)-π-*A*) is scarce, utilizing mostly azines such as pyridine [23–26] or triazine [27]. The DBT(O) may also be interconnected via various π-spacers to oligomeric chain [28]. Based on the observed nonlinear and fluorescent properties of DBT(O)-derived push-pull molecules, they were used as two photon absorbing (2 PA) materials for bioimaging and tested as active materials in OLED and OFET devices. Asymmetric DBT(O)-chromophores, e.g. those bearing peripheral triphenylamine donor and cyanoacrylic acceptor, were studied as sensitizers in DSSC [29].

* Corresponding author.
E-mail address: milan.klikar@upce.cz (M. Klikar).
URL: http://bures.upce.cz/klikar.html

https://doi.org/10.1016/j.tet.2019.07.017
0040-4020/

Despite a relatively large number of DBT(O) derivatives synthesized to date, it is quite surprising that DBT(O) has not been decorated by malonic acceptors so far. We have recently systematically explored malonic acid and their derivatives as electron withdrawing moieties focusing on their electronic features [30–32]. (Thio)barbituric acid has been identified as powerful acceptor with improved solubility due to possible *N*,*N*′-disubstitution. Hence, we focus our attention towards a series of chromophores **7**–**9** based on central DBT(O) unit and two peripheral barbituric acceptors connected via various π-spacers (Fig. 1). The target chromophores possess either electron donating DBT unit (A-π-D-π-A systems; series **a**) or electron withdrawing DBTO (A-π-A-π-A systems; series **b**). The length of the π-linker has also been adjusted – none (**7**), ethenylene (**8**) or ethynylene (**9**). The influence of the aforementioned structure changes on fundamental properties of **7**–**9** has experimentally been investigated by differential scanning calorimetry, cyclic voltammetry and electronic absorption spectroscopy completed by DFT calculations and nonlinear optical measurements. Based on the collected data, the structure-property relationships have been elucidated.

2. Results/discussion

2.1. Synthesis

The synthesis of all target chromophores started from commercially available dibenzothiophene **1** (Scheme 1). Upon its bromination [9] and oxidation [10], 2,8-dibromoDBT(O) **2a**–**b** were readily obtained. Twofold lithiation of dibromo derivatives **2a**–**b** followed by formylation with DMF [33] afforded dicarbaldehydes **3a**–**b**. Intermediates **2a**–**b** were also subjected to a twofold Sonogashira cross-coupling reaction with propargyl alcohol [30] providing DBT(O)-alcohols **5a**–**b**. The π-system of dicarbaldehydes **3a**–**b** was further extended via Wittig reaction with tributyl(1,3-dioxolan-2-ylmethyl)phosphonium bromide to afford **4a**–**b** exclusively as *E*-isomers [34]. Propargyl aldehydes **6a**–**b** were gained through a selective oxidation of alcohols **5a**–**b** using Dess-Martin reagent [35]. Despite a general excess of reagents has been used, the intermediates **3**–**6** were always partially contaminated by mono products, which were separated by column chromatography. Due to their planar arrangement and possible π-stacking, **3**–**6** are hardly soluble in common organic solvents, which also hampered their easy purification. For instance, aldehyde **4b** is almost insoluble. Hence, the attained yields mostly reflect purification issues rather than conversion of the reactions. With all aldehydes in hand, the final twofold Knoevenagel condensation with *N*,*N*′-dibutylbarbituric acid [31] was catalyzed by Al_2O_3 [36] providing target chromophores **7**–**9**. *N*,*N*′-Dibutylbarbituric acceptor ensured solubility of all target molecules but it also prevent their easy crystallization. All final molecules were purified by column chromatography. Whereas extended chromophores **8a** and **9a** were isolated in satisfactory yields of 71–78%, DBTO-analogues **8b** and **9b** showed certain instability during chromatography and, therefore, were gained in lower yields. Finally, all attempts to isolate and purify chromophores **7a**–**b**, with the barbituric moiety appended directly to the DBT(O), failed. The color change as well as TLC and HR-MALDI-MS analyses of the crude reaction mixture clearly confirmed presence of both **7a**–**b**. However their isolation as chemical individuals was not possible due to their reverse and ready decomposition to starting aldehydes **3a**–**b** and *N*,*N*′-dibutylbarbituric acid. We have observed such behavior already previously [30].

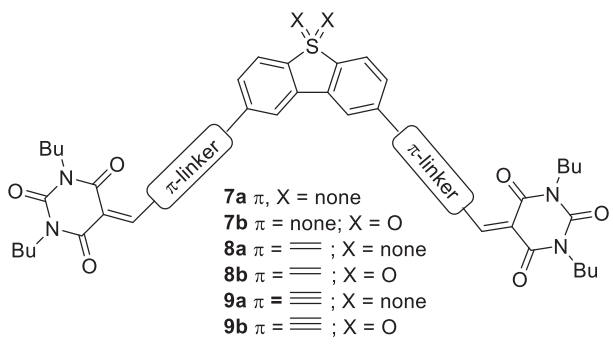

Fig. 1. General structural arrangements of target chromophores **7**–**9**.

2.2. Thermal properties

Thermal characteristics of target chromophores **8**–**9** as well as intermediates **3**–**6** were measured by differential scanning calorimetry (DSC). The measured melting points (T_m) and decomposition temperatures (T_d) are given in the experimental section. The DSC characteristics of target chromophores **8**–**9** were studied in detail with a scanning rate of 3 °C/min within the range of 25–400 °C (Fig. 2); the deduced T_m and T_d values are summarized in Table 1. Compounds **8a**–**b** with ethenylene π-linker exhibited sharp endothermic melting processes and gradual decomposition during further heating. On the contrary, a vigorous exothermic degradation without previous melting has been observed for **9a**–**b** with embedded triple bond. A monotropic solid-solid transition of metastable crystals (~175 °C) followed by melting of stable form has been observed for **8a**. As can be seen from the gathered data, compounds **8a**–**b** with embedded double bond showed significantly higher thermal robustness than ethynylene analogous **9a**–**b**. The thermal properties are also dictated by the DBT/DBTO central unit. The DBTO with two additional oxygen atoms brings increased thermal resistance as judged by both T_m and T_d values. Despite substituted with four butyl chains, **8b** possesses the melting point close to 250 °C. Compounds **9a**–**b** decomposed 100 °C below T_d of **8a**–**b**, their thermal behavior is clearly dictated by the presence of thermally labile ethynylene π-linker.

2.3. Electrochemistry

The electrochemical characterization of target chromophores **8**–**9** was carried out in acetonitrile containing 0.1 M Bu_4NPF_6 in a three electrode cell by cyclic voltammetry (CV). The acquired data are summarized in Table 1, CV diagrams are given in the SM. The first oxidations and reductions were determined as irreversible processes followed by subsequent oxidations within positive potentials. Although consecutive or simultaneous multiple-electron reductions can be assumed for chromophores with quadrupolar character, further reductions were not observed within the available negative potential window (Fig. S6). Based on judged peak currents $i_{p(ox1/red1)}$ for illustrative molecule **8a**, the first oxidations and reductions were likely recorded as one-electron processes; their potentials are clearly a function of the chromophore structure. It is assumed that the first reduction takes place at the barbituric acceptor. The first oxidation most likely involves either thiophene central donor (DBT) or is spread over entire π-conjugated system (DBTO). The peak potentials of the first oxidation $E_{p(ox1)}$ for DBTO-chromophores **8b**, and **9b** were not determined due to their localization out of the AcCN/Bu_4NPF_6 potential window. The deduced $E_{p(ox1)}$ and $E_{p(red1)}$ values were found within the range of 1.47–1.69 and −0.98 to −0.75 V, respectively. Due to unavailability of half-wave potentials, $E_{p(ox1)}$ and $E_{p(red1)}$ values were further recalculated to the HOMO/LUMO levels (Table 1) and are clearly

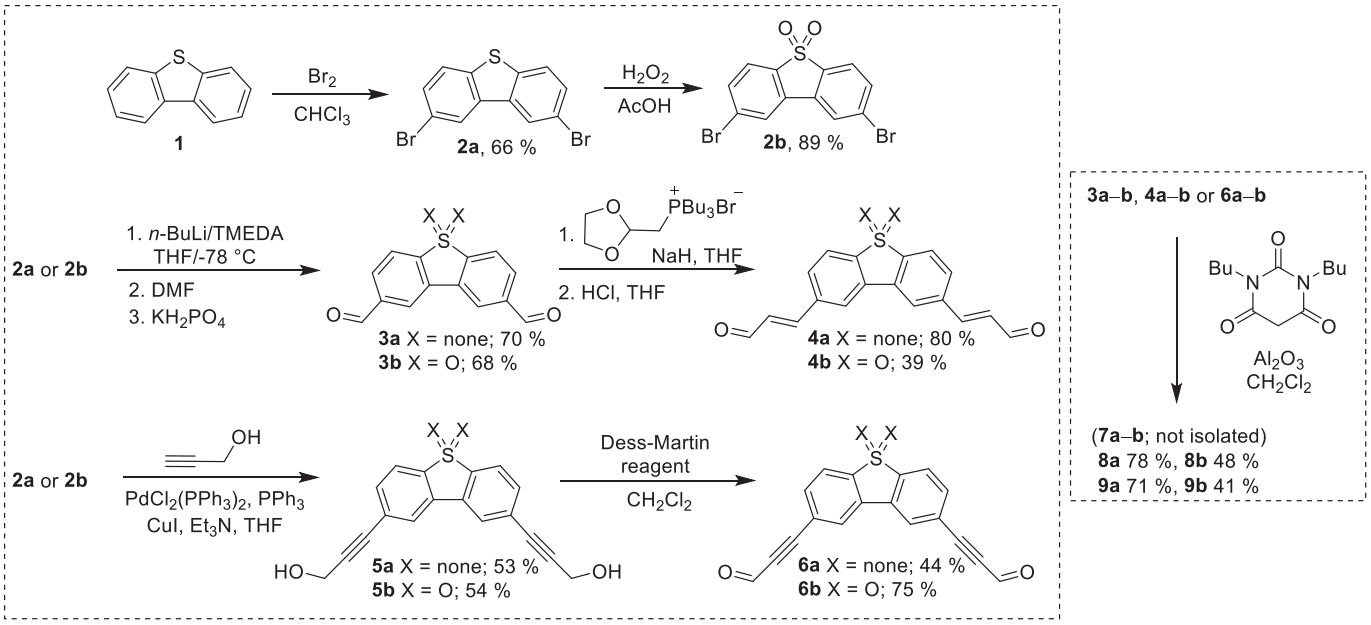

Scheme 1. Synthetic pathways leading to intermediate aldehydes **3**, **4** and **6** (left) and final Knoevenagel condensation to target chromophores **8**–**9** (right).

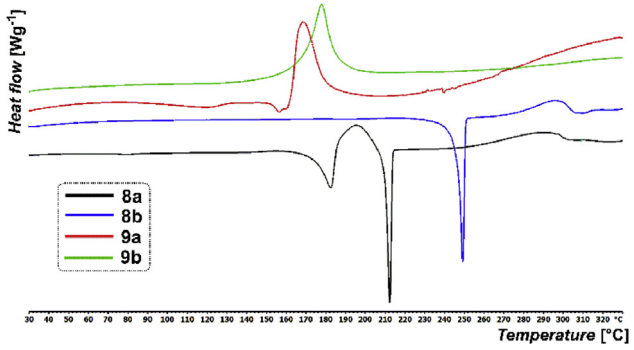

Fig. 2. DSC curves of chromophores **8**–**9** within the range of 25–330 °C.

visualized in energy level diagram (Fig. 3).

E_{LUMO} steadily decreases when going from **8** to **9** (π-system replacement) and from **a** to **b** (DBT→DBTO replacement). Significantly increased E_{HOMO} can be seen for A-π-D-π-A molecules **8a** and **9a** with DBT central donor. Suggesting the electrochemically determined HOMO levels similar to the calculated ones (Fig. 3), the opposite arrangement with central DBTO acceptor (**8b** and **9b**) brings deepened HOMO level and enlarged Δ*E*. Hence, chromophores **8a** and **9a** with DBT central donor showed the narrowest electrochemical gaps $\Delta E = 2.45/2.58$ eV. The effect of ethenylene→ethynylene π-linker replacement is less pronounced.

2.4. Optical absorption properties

Target chromophores **8**–**9** are yellow/orange solids, their linear optical properties were examined by UV-Vis spectroscopy in CH_2Cl_2. The literature shows, that DBT(O)-based molecules generally exhibit extraordinary fluorescent behavior. However, this is not the case of chromophores **8**–**9**, which showed very weak emission properties. We have observed previously that interconnection of barbituric acceptor with a donor/π-system quenches emission behavior [30–32]. The absorption spectra of four target chromophores are shown in Fig. 4; the longest-wavelength absorption maxima λ_{max} and the molar extinction coefficients ε_{max} are summarized in Table 1.

The longest-wavelength absorption maxima λ_{max} range from 349 to 434 nm with ε_{max} values of $45–67 \times 10^3\ M^{-1}\ cm^{-1}$. The spectra always exhibited one dominant band with an additional shoulder. The shoulder is either shifted hypsochromically (for A-π-D-π-A DBT-chromophores **8a** and **9a**) or bathochromically (for A-π-A-π-A systems **8b** and **9b**). This splitting of the absorption bands is due to a coupling between branches and reflects quadrupolar

Table 1
Fundamental properties of target chromophores **8**–**9**.

Comp.	T_m [°C][a]	T_d [°C][b]	$E_{p(ox1)}$ [V][c]	$E_{p(red1)}$ [V][c]	Δ*E* [eV][c]	E_{HOMO} [eV][d]	E_{LUMO} [eV][d]	λ^A_{max} [nm/eV][e]	ε^A_{max} [$10^3\ M^{-1}cm^{-1}$][e]	SHG [pmV^{-1}][f]	THG [a.u.][f]
8a	210	260	1.47	−0.98	2.45	−5.94	−3.49	404, 434/3.07, 2.86	53.1, 56.2	2.89	41
8b	247	270	–	−0.82	–	-	−3.65	359, 388/3.45, 3.19	66.8, 48.0	1.56	8
9a	–	160	1.69	−0.89	2.58	−6.16	−3.58	396, 427/3.13, 2.90	45.4, 49.4	2.83	35
9b	–	160	–	−0.75	–	-	−3.72	349, 383/3.55, 3.24	50.6, 32.9	1.21	6

[a] T_m = melting point (the point of intersection of a baseline and a tangent of thermal effect = onset).
[b] T_d = thermal decomposition (pyrolysis in N_2 atmosphere).
[c] $E_{p(ox1)}$ and $E_{p(red1)}$ are peak potentials of the first oxidation and reduction (irreversible processes), respectively, as measured by CV at scan rate 100 mVs^{-1}; all potentials are given *vs.* SSCE, $\Delta E = E_{p(ox1)} - E_{p(red1)}$.
[d] $-E_{HOMO/LUMO} = E_{p(ox1/red1)} + 4.429$ (in AcCN vs. SCE) [38] + 0.036 [difference between SCE (0.241 vs. SHE) and SSCE (0.205 vs. SHE)] [39].
[e] Measured in CH_2Cl_2 at $c \approx 1 \times 10^{-5}$ M.
[f] Second- and third-harmonic generations measured in oligoether acrylate at probing wavelength 1064 nm.

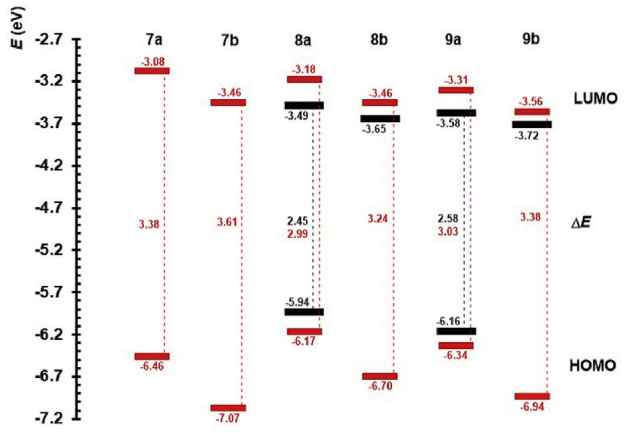

Fig. 3. Energy level diagram with electrochemical (black) and DFT calculated (red) HOMO/LUMO energies of chromophores **7**–**9**.

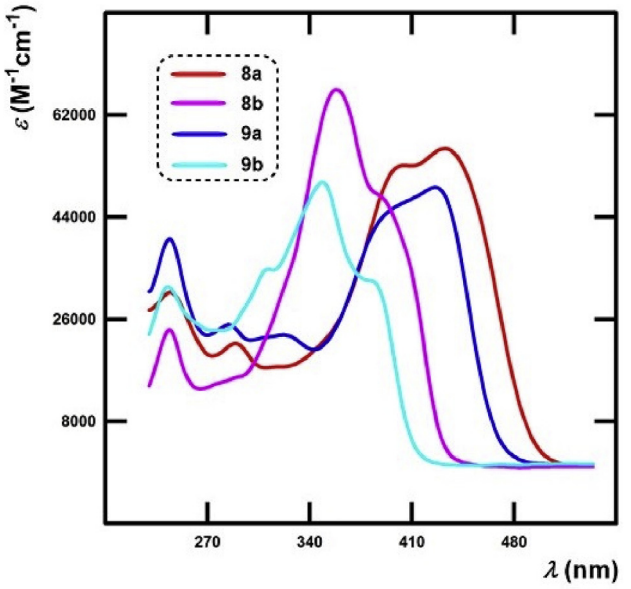

Fig. 4. UV-Vis absorption spectra of chromophores **8**–**9** measured in CH_2Cl_2 at $c \approx 1 \times 10^{-5}$ M.

arrangement of target chromophores. For V-shaped chromophores, the Frenkel exciton model predicts splitting of the singlet excited state into two bands positioned symmetrically with respect to the band of the corresponding linear D-π-A molecule [37]. As can be seen, the position of the bands are mainly dictated by the central unit. An apparent ICT from the central electron releasing DBT unit into two peripheral barbituric acceptors shifts the spectra of **8a** and **9a** bathochromically as compared to A-π-A-π-A systems **8b** and **9b** with DBTO central acceptor ($\Delta\lambda_{max} \approx 75$ nm/0.6 eV). The π-linker has less pronounced effect on the absorption spectra; a small difference ($\Delta\lambda_{max} = 5$–10 nm/$\approx$0.05 eV) has been found between chromophores **8** and **9** with ethenylene and ethynylene linkers, respectively. Hence, the spectra of chromophores **9a**–**b** are significantly hypsochromically and hypochromically shifted. In accordance with the electrochemical measurements, the most bathochromically shifted CT-band and the lowest optical gap have been measured for chromophore **8a**.

Solvatochromism of chromophores **8**–**9** was further investigated in nonpolar toluene and polar acetonitrile. The recorded spectra are depicted in Figs. S10–11 (see the SM) and the corresponding longest-wavelength absorption maxima are summarized in Table S1. As a general trend, all chromophores **8**–**9** showed slight hypsochromic shift with increasing the solvent polarity (toluene → CH_2Cl_2 → AcCN). It indicates that the ground state of these molecules is slightly more polar compared to the excited state regardless of their push-pull or pull-pull character.

2.5. Nonlinear optical properties

The nonlinear optical properties of chromophores **8**–**9** were explored by laser stimulated SHG and THG measurements. The powdered samples were embedded into the oligoether acrylate photopolymer matrices and were aligned in the dc-electric field using photo-solidification by a method similar to that we have used previously [40]. 5% $Nd^{3+}BiB_3O_6$ crystallites in powder form were used as reference samples. Pulsed Nd:YAG laser emitting at $\lambda = 1064$ nm with pulse duration of 8 ns and frequency repetition of 10 Hz was applied as a principal laser source, see the SM for detailed description of the experimental set-up. The principal dependence of the SHG versus the fundamental energy density for s-s polarization is shown in Fig. 5.

The obtained SHG data are slightly disturbed by the photothermal destruction and occurrence of laser stimulated absorption. The fluorescence contribution was spectrally separated by interference filters. Fig. 5 clearly shows that the highest experimental SHG efficiency was achieved for chromophore **9a**. The SHG nonlinear optical coefficients that take into account renormalization due to absorption (both linear and two-photon) as well as fluorescence are presented in Table 1. The experimental SHG responses were maximal for the DBT-derived dipolar chromophores **8a** and **9a** with A-π-D-π-A architecture. On the contrary, DBTO-derived chromophores **8b** and **9b** are less polarized with diminished SHG coefficients. The SHG measurements have also identified that chromophores **8a**–**b** with ethenylene linker possess slightly larger NLO activity than ethynylene analogues **9a**–**b** (Table 1). Compared to laser stimulated SHG efficiency of other organic chromophores measured at similar conditions, e.g. 2-(pyrene-1-yl) ethenylpyridine [41] or indolino-oxazolidine [42] derivatives, V-shaped chromophores **8** and **9** have demonstrated slightly better efficiency.

The third-order susceptibilities have been determined by maximal values of the THG versus the rotating angle and have been referenced to powdered $Y_3Al_5O_{12}$:Cr samples with known NLO susceptibilities [43]. The photo-thermal effect did not exceed

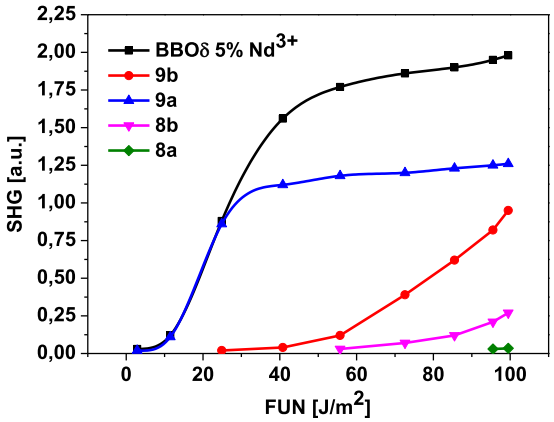

Fig. 5. Typical dependences of laser stimulated SHG of chromophores **8**–**9** vs. fundamental energy density.

5–7 K. An interference filter at 355 nm with the spectral width of about 10 nm with two additional interference filters at 345 and 365 nm, spectrally cutting the parasitic fluorescence scattered background, were employed to separate the reflected scattered signal from the NLO response. See the SM for more detailed description of the THG set-up. The typical dependences of the THG versus the fundamental 1064 nm ns pulsed beams are presented in Fig. 6. The evaluated values of the third-order susceptibilities vary within the range of 6–41 pm^2/V^2 (Table 1) and are comparable with the third-order optical nonlinearities of 8-hydroxyquinoline nickel complexes measured at similar condition [44]. Similar to SHG coefficients, the THG responses of chromophores **8**–**9** are affected by the central DBT/DBTO unit (**a** vs. **b**) as well as the ethenylene/ethynylene π-linkers (**8** vs. **9**). Whereas **8b** and **9b** showed diminished THG, the largest third-order NLO responses were recorded for **8a** and **9a**.

Using femtosecond laser at $\lambda = 1045$ nm with pulse duration 180 fs gives a similar dependences which imply that the role of the vibrational subsystem is not crucial here. The values of the photo induced NLO are relaxed up to the initial magnitudes within 1–2 min, which confirms a significant role of trapped metastable levels situated within forbidden energy gap. This will be a subject of a separate studies in a near future. However, the recorded photo induced changes of the second-order susceptibilities are higher than many other NLO-phores, e.g. inorganic-organic hybrid nanocomposites [45] or 4-(5-nitro-1,3-benzoxazol-2-yl)aniline derivatives [46].

2.6. Theoretical DFT calculations

Spatial and electronic properties of target chromophores were investigated using Gaussian®16W software [47] package at the DFT level. Initial geometries of molecules **7**–**9** were optimized by DFT B3LYP/6-311 + G(2df,p) method. Energies of the frontier molecular orbitals, their differences ΔE and ground state dipole moments μ were calculated at DFT B3LYP/6–311++G(2df,p) level in acetonitrile (AcCN). In order to accelerate the DFT calculations, butyl substituents of the barbituric moieties were replaced by methyls. The first hyperpolarizabilities β were computed at DFT B3LYP/6–311++G(2df,p) level in vacuum at 1064 nm. Theoretical electronic absorption spectra were calculated at TD-DFT (nstates = 8) B3LYP/6–311++G(2df,p) level in CH_2Cl_2 and corresponding λ_{max} values were deducted. All calculated data are summarized in Table 2 and Table S2.

The calculated HOMO and LUMO energies range from −7.07 to −6.17 and −3.56 to −3.08 eV and showed clear dependence on the structural arrangement of the particular chromophore as can be seen from the energy level diagram in Fig. 3. The LUMO energies, HOMO–LUMO and optical gaps correlate very tightly with the experimental data obtained by electrochemistry and UV-Vis spectra (see Figs. S14–S16 in the SM). The DFT calculations have identified similar structural features affecting fundamental properties of target chromophores; namely replacement of the central unit (DBT→DBTO) and presence/elongation of the π-linker. Hence, the widest and narrowest gaps have been calculated for A-π-A-π-A DBTO-chromophore **7b** without extended π-linker ($\Delta E = 3.61$ eV) and A-π-D-π-A DBT-chromophore **8a** with embedded double bonds ($\Delta E = 2.99$ eV). Based on the A-π-D-π-A character of DBT-chromophores, especially molecules **8a** and **9a** possess energetically quasi-degenerated LUMO and LUMO+1 (Fig. S13).

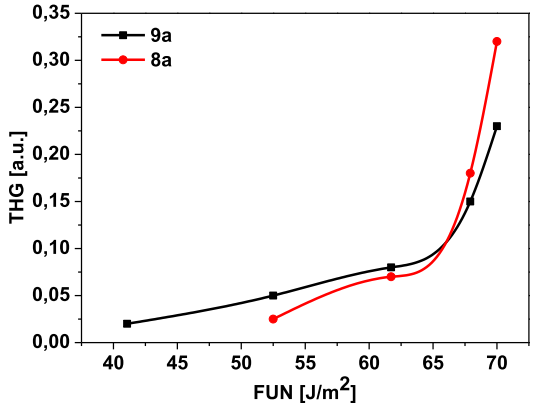

Fig. 6. Dependence of THG for chromophores **8a** and **9a** vs. fundamental energy density.

The HOMO/LUMO localizations were calculated at B3LYP/6–311++G(2df,p) level using DFT-optimized geometries and visualized in OPchem [48]. The frontier molecular orbitals in representative chromophores **9a** and **9b** are shown in Fig. 7; for complete listing see the SM. As expected, there is a clear HOMO/LUMO separation in push-pull chromophores in series **a** confirming their ICT character. Whereas the HOMO is centrally localized on the DBT donor, the LUMO is shifted towards both barbituric acceptors. The HOMO-1 and LUMO+1 are localized similarly. On the contrary, there is no HOMO/LUMO separation in A-π-A-π-A chromophores in series **b**. Both HOMO-1 and LUMO+1 are spread over the π-linker adjacent to the barbituric acceptors.

All target chromophores **7**–**9** possess C_{2v} group of symmetry with the ground state dipole moments μ between 2 and 5.5 D. DBT-chromophores in series **a** showed higher dipolar character than chromophores in series **b**. The calculated second-order polarizabilities β range from 24 to 302×10^{-30} esu and showed similar trends as the experimental SHG values. Push-pull DBT-chromophores in series **a** possess approximately four times larger β values in comparison to DBTO-analogues in series **b**. The β values also increases with elongation of the π-linker (**7** → **8**/**9**). However, almost identical hyperpolarizabilities were calculated for both pairs of chromophores with ethenylene/ethynylene π-linkers (**8a**/**9a** and **8b**/**9b**). Hence, the largest NLO coefficients β were calculated for chromophore **8a** (302×10^{-30} esu) and **9a** (298×10^{-30} esu).

Fig. 8 shows representative overlapped spectra of chromophore **8b**; for complete listing see the SM. The calculated λ_{max}^{DFT} values are listed in Table 2. Both experimental and calculated optical gaps ($1240/\lambda_{max}$) showed very tight correlation as shown in Fig. S16. Despite the TD-DFT spectra are slightly red-shifted ($\Delta\lambda_{max} \approx 40$ nm/0.25 eV), both spectra are almost identical with the same bands and shoulders. According to the analysis of the particular oscillators, the main band of DBT chromophores **7a**, **8a** and **9a** consists of the HOMO→LUMO transition. The hypsochromically shifted shoulders are originated from the HOMO−1→LUMO and HOMO−1→LUMO+1 transitions. For DBTO analogues **7b**, **8b** and **9b** is the situation completely opposite. The main band is created by the HOMO−1→LUMO and HOMO−1→LUMO+1 transitions, while the bathochromically shifted shoulder is generated by the HOMO→LUMO transition with a weaker oscillator strength.

3. Conclusion

Dibenzothiophene- and dibenzothiophene-*S*,*S*-dioxide-derived V-shaped chromophores with peripheral barbituric acceptors were designed and synthesized in a straightforward manner. The synthesis involved bromination and oxidation of commercially available dibenzothiophene and its subsequent modification via formylation, Wittig olefination, Sonogashira cross-coupling and final Knoevenagel condensation. Target chromophores with barbituric acceptors connected directly to DBT(O) central unit proved

Table 2
Principal DFT calculated characteristics of target chromophores **7**–**9**.

Comp.	E_{HOMO} [eV][a]	E_{LUMO} [eV][a]	ΔE [eV][a]	μ [D][a]	$\beta \times 10^{-30}$ [esu][b]	λ_{max}^{DFT} [nm/eV][c]	Group of symmetry
7a	−6.46	−3.08	3.38	3.95	85	425/2.92	C_{2v}
7b	−7.07	−3.46	3.61	4.43	24	399/3.11	C_{2v}
8a	−6.17	−3.18	2.99	5.37	302	478/2.59	C_{2v}
8b	−6.70	−3.46	3.24	3.37	73	434/2.86	C_{2v}
9a	−6.34	−3.31	3.03	5.56	298	472/2.63	C_{2v}
9b	−6.94	−3.56	3.38	1.98	71	420/2.95	C_{2v}

[a] Calculated at the DFT B3LYP/6−311++G(2df,p) level in AcCN.
[b] Calculated at the DFT B3LYP/6−311++G(2df,p) level in vacuum at 1064 nm (−2ω; ω,ω).
[c] Calculated at the TD-SCF (nstates = 8) B3LYP/6−311++G(2df,p) level in CH_2Cl_2.

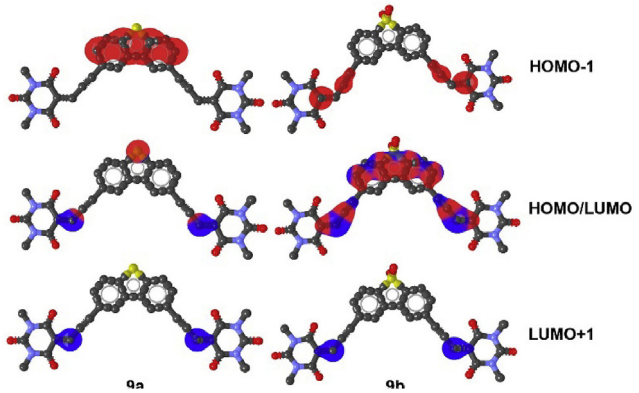

Fig. 7. The HOMO (red) an LUMO (blue) localizations in representative chromophores **9a** and **9b**.

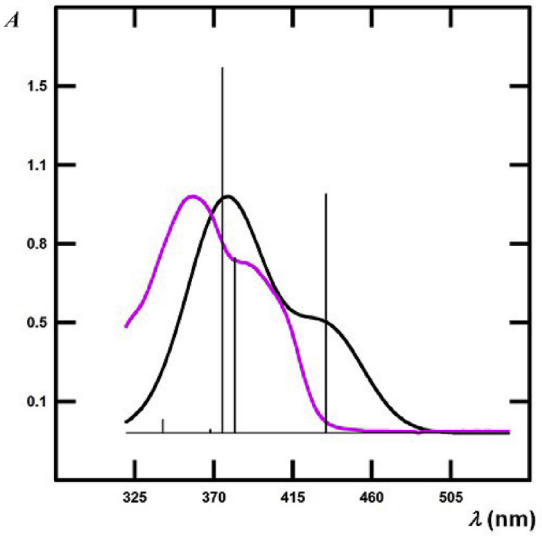

Fig. 8. The overlapped and fitted experimental (violet) and calculated (black) spectra of chromophore **8b**.

unstable. The fundamental thermal and optoelectronic properties were studied by DSC analysis and electrochemical and absorption spectra. It has been demonstrated that the used central donor (DBT) or acceptor (DBTO) as well as the ethenylene/ethynylene π-linkers affect the properties of chromophores **8** and **9** most significantly. The differences are mostly due to A-π-D-π-A (DBT) or A-π-A-π-A (DBTO) architecture of series **a** and **b**. These structural features also dictates the NLO responses of both chromophore types, the latter showed significantly diminished second- and third-order susceptibilities. The experimental data is further supported by DFT calculations. The lowest electrochemical/optical gaps and largest SHG and THG responses were measured for chromophores **8a** and **9a** based on the DBT central donor with A-π-D-π-A arrangement and ethenylene/ethynylene π-linkers.

4. Experimental section

4.1. General methods

Compounds **2a**–**b** and **3a** are known molecules. The preparation and characterization of dibromo derivatives **2a** and **2b** are given to the SM. The preparation of *N*,*N*′-dibutylbarbituric acid is carried out according our earlier procedure [31]. Starting DBT **1** as well as other reagents are commercially available. All commercial chemicals, reagents and solvents were purchased from suppliers such as Sigma Aldrich, TCI, Acros at reagent grade and were used as obtained. The dry THF was always freshly distilled from Na/K alloy and benzophenone under an inert atmosphere of argon. Formylation reaction, Wittig olefination and Sonogashira cross-coupling reaction were carried out in flame-dried flasks under argon. Column chromatography was carried out with silica gel 60 (particle size 0.040–0.063 mm, 230–400 mesh; Merck) and commercially available solvents. Thin-layer chromatography (TLC) was conducted on aluminum sheets coated with silica gel 60 F254, obtained from Merck, with visualization by a UV lamp (254 or 360 nm). Melting points of **2a**–**b** were determined by using Büchi B-540 instrument in open capillaries. Thermal properties of all remaining molecules were measured by differential scanning calorimetry with a Mettler-Toledo STARe System DSC 2/700 equipped with FRS 6 ceramic sensor and cooling system HUBER TC100-MT RC 23. The measurements were carried out in open aluminous crucibles under N_2 inert atmosphere. DSC curves were determined with a scanning rate of 3 °C/min within the range 25–400 °C for **8**–**9** and with a scanning rate of 10 °C/min within the range 100–400 °C for **3**–**6**. Melting point and temperature of decomposition were determined as intersection of baseline and tangent of peak (onset point). ^{1}H and ^{13}C NMR spectra were recorded at 400 and 100 MHz, respectively, with a Bruker AVANCE 400/500 instrument or 500 and 125 MHz, respectively, with Bruker Ascend™ 500 at 25 °C. Chemical shifts are reported in ppm relative to the signal of Me_4Si. The residual solvent signal in the ^{1}H and ^{13}C NMR spectra was used as an internal reference ($CDCl_3$ 7.25 and 77.25 ppm; DMSO-d_6 2.55 and 39.51 ppm). Apparent resonance multiplicities are described as s (singlet), d (doublet), dd (doublet of doublet), t (triplet) and m (multiplet); the coupling constants of multiplets (^3J or ^4J) are given in Hz. Mass spectra were measured with a GC-MS configuration comprised of an Agilent Technologies 6890 N gas chromatograph equipped with a 5973 Network MS detector (EI 70 eV, mass range 33–550 Da). High resolution MALDI MS spectra were measured on a MALDI mass spectrometer LTQ Orbitrap XL (Thermo Fisher

Scientific, Bremen, Germany) equipped with nitrogen UV laser (337 nm, 60 Hz). The LTQ Orbitrap instrument was operated in positive-ion mode over a normal mass range (*m/z* 50–2000) with resolution 100 000 at $m/z = 400$. The survey crystal positioning system (survey CPS) was set for the random choice of shot position by automatic crystal recognition. 2,5-Dihydroxybenzoic acid (DHB) was used as a matrix. Mass spectra were averaged over the whole MS record for all measured samples. The absorption spectra were measured on a Hewlett-Packard 8453 spectrophotometer in CH_2Cl_2 at 2×10^{-5} M. The electrochemical behavior of target chromophores were investigated by cyclic voltammetry in acetonitrile containing 0.1 M Bu_4NPF_6 in a three electrode cell by cyclic voltammetry (CV). The working electrode was glassy carbon disk (1 mm in diameter). Leak-less Ag/AgCl electrode (SSCE) containing filling electrolyte (3.4 M KCl) and titanium rod with a thick coating of platinum were used as the reference and auxiliary electrodes. All peak potentials are given *vs*. SSCE. Voltammetric measurements were performed by using an integrated potentiostat system ER466 (eDAQ Europe, Warszawa, Poland) operated with EChem Electrochemistry software.

4.2. General method A (formylation reaction)

The title compounds **3a**–**b** was synthesized via modified literature procedure [33]. Brominated derivative **2a** or **2b** (10 mmol) was dissolved in dry THF (150 mL) and the solution was cooled to −78 °C. Argon was bubbled through the solution for 15 min and TMEDA (3.0 mL, 20 mmol) followed by *n*-BuLi (13.75 mL 1.6 M in hexane, 22 mmol) were added dropwise. The reaction mixture was stirred at −78 °C for 90 min. DMF (3.9 mL, 50 mmol) was added and the reaction mixture was stirred at room temperature for 24 h. The reaction mixture was quenched with saturated solution of KH_2PO_4 (150 mL) and extracted with EtOAc (3 × 150 mL). The combined organic fractions were dried (Na_2SO_4) and the solvents were removed in *vacuo*. The crude product **3a** or **3b** was purified by column chromatography (SiO_2, CH_2Cl_2/EtOAc 25:1).

4.3. General method B (Wittig olefination)

The compounds **4a**–**b** were synthesized via modified literature procedure [34]. Aldehyde **3a** or **3b** (2 mmol) and tributyl(1,3-dioxolan-2-ylmethyl)phosphonium bromide (1.63 g, 4.4 mmol) were dissolved in dry THF (50 mL). Argon was bubbled through the solution for 15 min, NaH (144 mg, 6 mmol) was added and the reaction mixture was stirred at room temperature for 24 h. The reaction mixture was diluted with water (100 mL) and extracted with EtOAc (3 × 100 mL). The combined organic layers were dried (Na_2SO_4) and the solvents were evaporated in *vacuo*. The residue was dissolved in THF (100 mL), 12% HCl (50 mL) was added and the solution was stirred for 1 h. The reaction mixture was diluted with water (100 mL) and extracted with EtOAc (3 × 100 mL). Both products **4a** and **4b** are sparingly soluble in common organic solvents. Therefore, the collected organic suspensions was concentrated in *vacuo* and precipitate was filtered off. The crude product **4a** or **4b** was suspended in EtOAc (50 mL), the suspension was refluxed for 30 min, cooled to 25 °C and the product was isolated by filtration. After drying, products **4a** and **4b** were used in the following reaction step without further purification. A full purification of small quantities is possible by column chromatography (SiO_2, CH_2Cl_2/EtOAc 10:1) using large excess of the eluting solvents.

4.4. General method C (Sonogashira cross-coupling reaction)

The compounds **5a**–**b** were synthesized via modified literature procedure [30]. Brominated derivative **2a** or **2b** (3 mmol) and propargyl alcohol (0.7 mL, 12 mmol) were dissolved in dried solution of THF/Et_3N (100:25 mL). Argon was bubbled through the solution for 15 min, whereupon $[PdCl_2(PPh_3)_2]$ (105 mg, 0.15 mmol), PPh_3 (39 mg, 0.15 mmol) and CuI (57 mg, 0.3 mmol) were added, and the reaction mixture was stirred under argon at 60 °C for 24 h. The solvents were evaporated and the crude product was extracted portioned between NH_4Cl (100 mL) and CH_2Cl_2 (3 × 100 mL). The combined organic extracts were dried (Na_2SO_4) and the solvents were evaporated *in vacuo*. The crude product **5a** or **5b** was purified by column chromatography (SiO_2, CH_2Cl_2/EtOAc 1:1) or precipitated from CH_2Cl_2 solution with hexane.

4.5. General method D (Dess-Martin oxidation)

The compounds **6a**–**b** were synthesized via modified literature procedure [35]. Alcohol **5a** or **5b** (2 mmol) and Dess-Martin periodinane (1.87 g, 4.4 mmol) were suspended in CH_2Cl_2 (200 mL). The reaction mixture was stirred at 25 °C for 24 h, diluted with water (100 mL) and extracted with CH_2Cl_2 (2 × 100 mL). The combined organic layers were dried (Na_2SO_4) and the solvent was removed in *vacuo*. The crude product **6a** or **6b** was purified by column chromatography (SiO_2, CH_2Cl_2/EtOAc 25:1).

4.6. General method E (Knoevenagel condensation)

The final chromophores **8a**–**b** or **9a**–**b** were synthesized via modified literature procedure [36]. Aldehyde **4a**, **4b**, **6a** or **6b** (0.5 mmol) and *N*,*N*′-dibutylbarbituric acid (360 mg, 1.5 mmol) were dissolved in CH_2Cl_2 (75 mL) and Al_2O_3 (510 mg, 5 mmol, Brockmann II-III) was added. The reaction mixture was stirred at 25 °C for 24 h. Al_2O_3 was filtered off and the filtrate was evaporated in *vacuo*. The crude product was purified by column chromatography (SiO_2, CH_2Cl_2/EtOAc 50:1).

4.7. Dibenzo[b,d]thiophene-2,8-dicarbaldehyde (*3a*)

The title compound was prepared from bromo derivative **2a** (3.42 g) following the general procedure A. The product **3a** was obtained as a white solid (1.68 g, 70%; Ref. [33] 75%). $R_f = 0.65$ (CH_2Cl_2); $T_m = 235$ °C (Ref. [49] 233–234 °C), $T_d > 340$ °C. EI-MS (70 eV) *m/z* (rel. int.): 240 ($[M]^+$, 100), 211 (41), 182 (25), 139 (30). ^{1}H NMR (500 MHz, 25 °C, DMSO-d_6): $\delta = 8.10$ (dd, $J_1 = 8$ Hz, $J_2 = 1.5$ Hz, 2H, CH_{AR}), 8.36 (d, $J = 8.5$ Hz, 2H, CH_{AR}), 8.72 (s, 2H, CH_{AR}), 9.10 (d, $J = 1$ Hz, 2H, CH_{AR}), 10.21 ppm (s, 2H, CH=O). ^{13}C NMR (125 MHz, 25 °C, $CDCl_3$): $\delta = 123.82$; 124.18; 127.87; 133.92; 135.58; 146.31; 191.66 ppm.

4.8. 5,5-Dioxo-5H-5λ^6-dibenzo[b,d]thiophene-2,8-dicarbalde-hyde (*3b*)

The title compound was prepared from bromo derivative **2b** (3.74 g) following the general procedure A. The product was obtained as a yellowish solid (1.85 g, 68%). $R_f = 0.45$ (CH_2Cl_2); $T_m = 320$ °C, $T_d > 360$ °C. EI-MS (70 eV) *m/z* (rel. int.): 272 ($[M]^+$, 100), 215 (73), 150 (42), 115 (35). ^{1}H NMR (500 MHz, 25 °C, DMSO-d_6): $\delta = 8.26$ (dd, $J_1 = 8$ Hz, $J_2 = 1$ Hz, 2H, CH_{AR}), 8.35 (d, $J = 8$ Hz, 2H, CH_{AR}), 8.92 (s, 2H, CH_{AR}), 10.21 ppm (s, 2H, CH=O). ^{13}C NMR (125 MHz, 25 °C, DMSO-d_6): $\delta = 123.17$; 123.80; 131.04; 132.83; 140.83; 140.92; 192.05 ppm.

4.9. (2E,2′E)-3,3′-(Dibenzo[b,d]thiene-2,8-diyl)di(prop-2-enal) (*4a*)

The title compound was prepared from aldehyde **3a** (480 mg) following the general procedure B. The product **4a** was obtained as a yellowish solid (467 mg, 80%). $R_f = 0.50$ (CH_2Cl_2/EtOAc 20:1);

$T_m = 260\,^{\circ}C$, $T_d > 320\,^{\circ}C$. ^1H NMR (500 MHz, 25 °C, DMSO-d_6): $\delta = 7.16$ (dd, $J_1 = 16$ Hz, $J_2 = 8$ Hz, 2H, CH), 7.94–7.97 (m, 4H, CH + CH_{AR}), 8.23 (d, $J = 8.5$ Hz, 2H, CH_{AR}), 9.10 (d, $J = 1$ Hz, 2H, CH_{AR}), 9.81 ppm (d, $J = 8$ Hz, 2H, CH═O). ^{13}C NMR (125 MHz, 25 °C, DMSO-d_6): $\delta = 122.58$; 124.33; 128.68; 129.01; 131.74; 135.85; 142.43; 153.46; 194.98 ppm. HR-FT-MALDI-MS (DHB) *m/z*: calculated for $C_{18}H_{13}O_2S^+$ ($[M+H]^+$): 293.06308; found 293.06512.

4.10. (2E,2'E)-3,3'-(5,5-Dioxo-5H-5λ^6-dibenzo[b,d]thiene-2,8-di-yl) di(prop-2-enal) (**4b**)

The title compound was prepared from aldehyde **3b** (544 mg) following the general procedure B. After filtration step, the column chromatography was employed to separate mono product. The product **4b** was obtained as a yellowish solid (253 mg, 39%). $R_f = 0.20$ (CH_2Cl_2/EtOAc 20:1); $T_d > 350\,^{\circ}C$. ^1H NMR (500 MHz, 25 °C, DMSO-d_6): $\delta = 7.19$ (dd, $J_1 = 16$ Hz, $J_2 = 7.5$ Hz, 2H, CH), 7.93 (d, $J = 15.5$ Hz, 2H, CH), 8.03 (d, $J = 8$ Hz, 2H, CH_{AR}), 8.19 (d, $J = 7.5$ Hz, 2H, CH_{AR}), 8.83 (s, 2H, CH_{AR}), 9.84 ppm (d, $J = 7.5$ Hz, 2H,CH═O). ^{13}C NMR (125 MHz, 25 °C, DMSO-d_6): $\delta = 121.78$; 123.09; 131.43; 131.52; 132.65; 138.55; 140.40; 150.60; 194.88 ppm. HR-FT-MALDI-MS (DHB) *m/z*: calculated for $C_{18}H_{13}O_4S^+$ ($[M+H]^+$): 325.05291; found 325.05329.

4.11. 3,3'-(Dibenzo[b,d]thiene-2,8-diyl)di(prop-2-yn-1-ol) (**5a**)

The title compound was prepared from bromo derivative **2a** (1.026 g) following the general procedure C. The product was obtained as a light ocher solid (465 mg, 53%). $R_f = 0.60$ (CH_2Cl_2/EtOAc 1:1); $T_d > 200\,^{\circ}C$. ^1H NMR (500 MHz, 25 °C, DMSO-d_6): $\delta = 4.41$ (d, $J = 6$ Hz, 4H, CH_2), 5.47 (t, $J = 6$ Hz, 2H, OH), 7.61 (dd, $J_1 = 8$ Hz, $J_2 = 1$ Hz, 2H, CH_{AR}), 8.11 (d, $J = 8.5$ Hz, 2H, CH_{AR}), 8.61 ppm (d, $J = 0.5$ Hz, 2H, CH_{AR}). ^{13}C NMR (125 MHz, 25 °C, DMSO-d_6): $\delta = 49.54$; 83.66; 90.06; 119.11; 123.45; 125.26; 130.17; 134.67; 139.08 ppm. HR-FT-MALDI-MS (DHB) *m/z*: calculated for $C_{18}H_{12}O_2S^+$ ($[M]^+$): 292.05525; found 292.05556.

4.12. 2,8-Bis(3-hydroxyprop-1-yn-1-yl)-5H-5λ^6-dibenzo[b,d]thiophene-5,5-dione) (**5b**)

The title compound was prepared from bromo derivative **2b** (1.122 mg) following the general procedure C. The product was obtained as a light ocher solid (525 mg, 54%). $R_f = 0.40$ (CH_2Cl_2/EtOAc 1:1); $T_d > 210\,^{\circ}C$. ^1H NMR (500 MHz, 25 °C, DMSO-d_6): $\delta = 4.43$ (d, $J = 6$ Hz, 4H, CH_2), 5.57 (t, $J = 6$ Hz, 2H, OH), 7.73 (d, $J = 8$ Hz, 2H, CH_{AR}), 8.06 (d, $J = 8$ Hz, 2H, CH_{AR}), 8.47 ppm (s, 2H, CH_{AR}). ^{13}C NMR (125 MHz, 25 °C, DMSO-d_6): $\delta = 49.46$; 82.27; 94.07; 122.47; 125.86; 128.69; 130.82; 133.92; 136.26 ppm. HR-FT-MALDI-MS (DHB) *m/z*: calculated for $C_{18}H_{13}O_4S^+$ ($[M+H]^+$): 325.05291; found 325.05329.

4.13. 3,3'-(Dibenzo[b,d]thiene-2,8-diyl)di(prop-2-ynal)(**6a**)

The title compound was prepared from alcohol **5a** (584 mg) following the general procedure D. The product was obtained as a light orange solid (253 mg, 44%). $R_f = 0.85$ (CH_2Cl_2); $T_d > 215\,^{\circ}C$. ^1H NMR (500 MHz, 25 °C, DMSO-d_6): $\delta = 7.89$ (dd, $J_1 = 8.5$ Hz, $J_2 = 1.5$ Hz, 2H, CH_{AR}), 8.31 (d, $J = 8.5$ Hz, 2H, CH_{AR}), 9.04 (d, $J = 1$ Hz, 2H, CH_{AR}), 9.55 ppm (s, 2H, CH═O). ^{13}C NMR (100 MHz, 25 °C, $CDCl_3$): $\delta = 89.10$; 95.01; 116.31; 123.64; 127.16; 131.77; 134.98; 143.10; 176.84 ppm. HR-FT-MALDI-MS (DHB) *m/z*: calculated for $C_{18}H_9O_2S^+$ ($[M+H]^+$): 289.03178; found 289.03193.

4.14. 3,3'-(5,5-Dioxo-5H-5λ^6-dibenzo[b,d]thiene-2,8-diyl)di(prop-2-ynal) (**6b**)

The title compound was prepared from alcohol **5b** (648 mg) following the general procedure D. The product was obtained as a light ocher solid (480 mg, 75%). $R_f = 0.60$ (CH_2Cl_2); $T_d > 230\,^{\circ}C$. ^1H NMR (400 MHz, 25 °C, DMSO-d_6): $\delta = 8.04$ (d, $J = 7.6$ Hz, 2H, CH_{AR}), 8.24 (d, $J = 8$ Hz, 2H, CH_{AR}), 8.77 (s, 2H, CH_{AR}), 9.56 ppm (s, 2H, CH═O). ^{13}C NMR (125 MHz, 25 °C, DMSO-d_6): $\delta = 89.82$; 90.28; 123.03; 125.00; 127.82; 130.65; 135.80; 138.45; 178.75 ppm. HR-FT-MALDI-MS (DHB) *m/z*: calculated for $C_{18}H_9O_4S^+$ ($[M+H]^+$): 321.02161; found 321.02234.

4.15. DBT-chromophore (**8a**)

The title chromophore was prepared from aldehyde **4a** (146 mg) following the general procedure E. The product was obtained as a bright orange solid (287 mg, 78%). $R_f = 0.80$ (CH_2Cl_2/Hexane 3:1); $T_m = 210\,^{\circ}C$; $T_d > 260\,^{\circ}C$. ^1H NMR (500 MHz, 25 °C, $CDCl_3$): $\delta = 0.94$–0.99 (m, 12H, CH_3), 1.35–1.45 (m, 8H, CH_2), 1.60–1.68 (m, 8H, CH_2), 3.94–3.97 (m, 8H, CH_2), 7.56 (d, $J = 15$ Hz, 2H, CH), 7.83–7.88 (m, 4H, 2 × CH_{AR}), 8.22 (d, $J = 12$ Hz, 2H, CH), 8.37 (s, 2H, CH_{AR}), 8.70 ppm (dd, $J_1 = 15.5$ Hz, $J_2 = 12$ Hz, 2H, CH). ^{13}C NMR (125 MHz, 25 °C, $CDCl_3$): $\delta = 14.00$; 14.04; 20.39; 20.49; 30.36; 30.43; 41.73; 42.23; 114.88; 123.25; 123.73; 125.47; 127.26; 132.66; 135.38; 143.24; 151.12; 153.73; 157.14; 161.81; 162.24 ppm. HR-FT-MALDI-MS (DHB) *m/z*: calculated for $C_{42}H_{49}N_4O_6S^+$ ($[M+H]^+$): 737.33226; found 737.33669.

4.16. DBTO-chromophore (**8b**)

The title chromophore was prepared from aldehyde **4b** (162 mg) following the general procedure E. The product was obtained as a yellow solid (185 mg, 48%). $R_f = 0.95$ (CH_2Cl_2/EtOAc 20:1); $T_m = 247\,^{\circ}C$; $T_d > 270\,^{\circ}C$. ^1H NMR (500 MHz, 25 °C, $CDCl_3$): $\delta = 0.94$–0.99 (m, 12H, CH_3); 1.35–1.44 (m, 8H, CH_2), 1.58–1.67 (m, 8H, CH_2), 3.95–3.98 (m, 8H, CH_2), 7.45 (d, $J = 16$ Hz, 2H, CH), 7.85–7.89 (m, 4H, 2 × CH_{AR}), 8.09 (s, 2H, CH_{AR}), 8.19 (d, $J = 12$ Hz, 2H, CH), 8.74 ppm (dd, $J_1 = 16$ Hz, $J_2 = 12$ Hz, 2H, CH). ^{13}C NMR (125 MHz, 25 °C, $CDCl_3$): $\delta = 13.99$; 14.03; 20.37; 20.47; 30.32; 30.39; 41.90; 42.41; 117.26; 121.84; 123.18; 128.59; 130.99; 132.07; 139.34; 141.25; 149.71; 150.89; 155.41; 161.53; 161.82 ppm. HR-FT-MALDI-MS (DHB) *m/z*: calculated for $C_{42}H_{49}N_4O_8S^+$ ($[M+H]^+$): 769.32656; found 769.32741.

4.17. DBT-chromophore (**9a**)

The title chromophore was prepared from aldehyde **6a** (144 mg) following the general procedure E. The product was obtained as a bright yellow solid (260 mg, 71%). $R_f = 0.80$ (CH_2Cl_2/Hexane 3:1); $T_d > 160\,^{\circ}C$. ^1H NMR (500 MHz, 25 °C, $CDCl_3$): $\delta = 0.94$–0.99 (m, 12H, CH_3); 1.36–1.44 (m, 8H, CH_2), 1.61–1.69 (m, 8H, CH_2), 3.94–4.00 (m, 8H, CH_2), 7.80 (dd, $J_1 = 8.5$ Hz, $J_2 = 1.5$ Hz, 2H, CH_{AR}), 7.84 (s, 2H, CH), 7.91 (d, $J = 8$ Hz, 2H, CH_{AR}), 8.49 ppm (d, $J = 1$ Hz, 2H, CH_{AR}). ^{13}C NMR (125 MHz, 25 °C, $CDCl_3$): $\delta = 13.97$; 14.03; 20.36; 20.43; 30.30; 30.33; 41.90; 42.41; 90.62; 117.45; 118.68; 123.48; 125.67; 127.21; 132.11; 135.22; 136.25; 143.01; 150.82; 159.40; 161.23 ppm. HR-FT-MALDI-MS (DHB) *m/z*: calculated for $C_{42}H_{45}N_4O_6S^+$ ($[M+H]^+$): 733.30543; found 733.30634.

4.18. DBTO-chromophore (**9b**)

The title chromophore was prepared from aldehyde **6b** (160 mg) following the general procedure E. The product was obtained as a dark yellow solid (157 mg, 41%). $R_f = 0.95$ (CH_2Cl_2/EtOAc 20:1);

$T_d > 160$ °C. ^{1}H NMR (500 MHz, 25 °C, $CDCl_3$): $\delta = 0.94–0.98$ (m, 12H, CH_3); 1.34–1.43 (m, 8H, CH_2), 1.59–1.67 (m, 8H, CH_2), 3.94–3.97 (m, 8H, CH_2), 7.76 (s, 2H, CH), 7.84–7.89 (m, 4H, $2 \times CH_{AR}$), 8.07 ppm (s, 2H, CH_{AR}). ^{13}C NMR (125 MHz, 25 °C, $CDCl_3$): $\delta = 13.95$; 14.00; 20.33; 20.39; 30.25; 30.27; 42.03; 42.54; 91.56; 111.85; 122.85; 126.06; 127.66; 128.06; 131.28; 134.62; 135.61; 138.97; 150.55; 159.07; 160.72 ppm. HR-FT-MALDI-MS (DHB) *m/z*: calculated for $C_{42}H_{45}N_4O_8S^+$ ($[M+H]^+$): 765.29526; found 765.29637.

Acknowledgments

For I. V. Kityk and J. Jedyrka the presented results are the part of a project that has received funding from the European Union's Horizon 2020 research and innovation program under the Marie Skłodowska-Curie grant agreement No. 778156. Supported from resources for science in years 2018–2022 granted for the realization of international co-financed project No. W13/H2020/2018 (Dec. MNiSW 3871/H2020/2018/2) is also acknowledged.

Appendix A. Supplementary data

Supplementary data to this article can be found online at https://doi.org/10.1016/j.tet.2019.07.017.

References

[1] M.E. Forrest, S.R. Thompson, Organic electronics and optoelectronics, Chem. Rev. 107 (2007) 923–1386.
[2] E.A. Miller, R.D. Chandross, Materials for electronics, Chem. Rev. 110 (2010) 1–574.
[3] P.N. He, G.S. Tan, L.S. Zheng, Q. Prasad, Multiphoton absorbing Materials: molecular designs, characterizations, and applications, Chem. Rev. 108 (2008) 1245–1330, https://doi.org/10.1021/cr050054x.
[4] Y. Ohmori, Development of organic light-emitting diodes for electro-optical integrated devices, Laser Photonics Rev. 4 (2010) 300–310, https://doi.org/10.1002/lpor.200810059.
[5] F. Bureš, Fundamental aspects of property tuning in push-pull molecules, RSC Adv. 4 (2014) 58826–58851, https://doi.org/10.1039/c4ra11264d.
[6] D.F. Perepichka, I.F. Perepichka, Handbook of Thiophene-Based Materials: Applications in Organic Electronics and Photonics, John Wiley & Sons, Ltd, 2009, https://doi.org/10.1002/9780470745533.
[7] J. Podlesný, O. Pytela, M. Klikar, V. Jelínková, I.V. Kityk, K. Ozga, J. Jedryka, M. Rudysh, F. Bureš, Small isomeric push–pull chromophores based on thienothiophenes with tunable optical (non)linearities, Org. Biomol. Chem. 17 (2019) 3623–3634, https://doi.org/10.1039/C9OB00487D.
[8] C.C. Ashby, J. Cook, Recent advances in the chemistry of dibenzothiophenes, Adv. Heterocycl. Chem. 16 (1974) 181–288, https://doi.org/10.1016/b978-0-08-025256-8.50013-9.
[9] Q. Hou, W. Yang, C. Liu, R. Yang, Y. Cao, J. Huang, Y. Niu, Improvement of color purity in blue-emitting polyfluorene by copolymerization with dibenzothiophene, J. Mater. Chem. 13 (2003) 1351–1355, https://doi.org/10.1039/b300202k.
[10] T. Shan, P. Lu, X. Tang, X. He, Q. Bai, H. Ma, Efficient deep-blue electroluminescence based on phenanthroimidazole-dibenzothiophene derivatives with different oxidation states of the sulfur atom, Chem. Asian J. 12 (2017) 552–560, https://doi.org/10.1002/asia.201601626.
[11] A. Liang, M. Luo, Y. Liu, H. Wang, Z. Wang, X. Zheng, T. Cao, D. Liu, Y. Zhang, F. Huang, Novel yellow phosphorescent iridium complexes with dibenzothiophene-S,S-dioxide-based cyclometalated ligand for white polymer light-emitting diodes, Dyes Pigments 159 (2018) 637–645, https://doi.org/10.1016/j.dyepig.2018.07.019.
[12] K.C. Moss, K.N. Bourdakos, V. Bhalla, K.T. Kamtekar, M.R. Bryce, M.A. Fox, H.L. Vaughan, F.B. Dias, A.P. Monkman, Tuning the intramolecular charge transfer emission from deep blue to green in ambipolar systems based on dibenzothiophene S,S-dioxide by manipulation of conjugation and strength of the electron donor units, J. Org. Chem. 75 (2010) 6771–6781, https://doi.org/10.1021/jo100898a.
[13] S. Kumar, S. Patil, High T_g fluoranthene-based electron transport materials for organic light-emitting diodes, New J. Chem. 39 (2015) 6351–6357, https://doi.org/10.1039/c5nj00750j.
[14] Y.S. Kim, J.Y. Yoon, H.W. Lee, J. Kim, H.W. Lee, S.E. Lee, Y.K. Kim, S.S. Yoon, Blue fluorescent materials based on bis(10-phenylanthracen-9-yl) derivatives containing heterocyclic moiety, Opt. Mater. (Amst.) 46 (2015) 247–253, https://doi.org/10.1016/j.optmat.2015.04.027.
[15] W. Huang, M. Jiang, S. Qian, B. Li, X. Wang, P. Yang, W. Jiang, X. Tao, Two-photon absorption of new multibranched chromophore with dibenzothiophene core, Chem. Phys. Lett. 424 (2006) 333–339, https://doi.org/10.1016/j.cplett.2006.04.099.
[16] T.H. Huang, W.T. Whang, J.Y. Shen, J.T. Lin, H. Zheng, Organic electroluminescent derivatives containing dibenzothiophene and diarylamine segments, J. Mater. Chem. 15 (2005) 3233–3240, https://doi.org/10.1039/b507210g.
[17] T.H. Huang, J.T. Lin, L.Y. Chen, Y.T. Lin, C.C. Wu, Dipolar dibenzothiophene S,S-dioxide derivatives containing diarylamine: materials for single-layer organic light-emitting devices, Adv. Mater. 18 (2006) 602–606, https://doi.org/10.1002/adma.200502078.
[18] J.H. Kim, J.Y. Lee, Dibenzothiophene-dioxide acceptor based thermally activated delayed fluorescent emitters for color tunable organic light-emitting diodes, J. Ind. Eng. Chem. 50 (2017) 111–114, https://doi.org/10.1016/j.jiec.2017.02.001.
[19] S.H. Hsiao, L.C. Wu, Fluorescent and electrochromic polymers from 2,8-di(carbazol-9-yl)dibenzothiophene and its S,S-dioxide derivative, Dyes Pigments 134 (2016) 51–63, https://doi.org/10.1016/j.dyepig.2016.06.043.
[20] Z. Chen, J. Ye, C. Zheng, C.S. Lee, Y. Yuan, X. Ou, X. Zhang, M.K. Fung, Carbazole/sulfone hybrid D-π-A-structured bipolar fluorophores for high-efficiency blue-violet electroluminescence, Chem. Mater. 25 (2013) 2630–2637, https://doi.org/10.1021/cm400945h.
[21] J.H. Kim, S.H. Han, J.Y. Lee, Dibenzothiophene derived hosts with CN substituted carbazole for blue thermally activated delayed fluorescent organic light-emitting diodes, Synth. Met. 232 (2017) 152–158, https://doi.org/10.1016/j.synthmet.2017.08.014.
[22] J. Gao, L. Li, Q. Meng, R. Li, H. Jiang, H. Li, W. Hu, Dibenzothiophene derivatives as new prototype semiconductors for organic field-effect transistors, J. Mater. Chem. 17 (2007) 1421–1426, https://doi.org/10.1039/b616381e.
[23] X.J. Feng, P.L. Wu, F. Bolze, H.W.C. Leung, K.F. Li, N.K. Mak, D.W.J. Kwong, J.F. Nicoud, K.W. Cheah, M.S. Wong, Cyanines as new fluorescent probes for DNA detection and two-photon excited bioimaging, Org. Lett. 12 (2010) 2194–2197, https://doi.org/10.1021/ol100474b.
[24] S. Chi, L. Li, Y. Wu, A series of novel dibenzothiophene-based two-photon fluorescent probes for cellular nucleus imaging, Sens. Actuators B Chem. 231 (2016) 811–829, https://doi.org/10.1016/j.snb.2016.03.006.
[25] S. Chi, L. Li, Y. Wu, Novel mono-cationic fluorescent probes based on different central π-conjugated bridges for two-photon bioimaging of cellular nuclei, RSC Adv. 6 (2016) 69748–69757, https://doi.org/10.1039/c6ra12193d.
[26] C.Y. Huang, J. Wang, Z.Y. Ding, K. Cui, Luminescent properties, internal hydrogen bonds and π-π Interactions of Cd(II), Zn(II), Co(II) complexes based on 2,8-di(pyridin-4-yl)dibenzothiophene and dicarboxylate ligands, J. Mol. Struct. 1086 (2015) 118–124, https://doi.org/10.1016/j.molstruc.2015.01.020.
[27] Y.J. Kang, J.Y. Lee, High triplet energy electron transport type exciton blocking materials for stable blue phosphorescent organic light-emitting diodes, Org. Electron. Phys. Mater. Appl. 32 (2016) 109–114, https://doi.org/10.1016/j.orgel.2016.02.025.
[28] K.L. Pik, F.L. King, S.W. Man, W.C. Kok, Synthesis and structure-linear and structure-nonlinear optical properties of multi-dipolar zigzag oligoaryleneethynylenes, J. Org. Chem. 72 (2007) 6672–6679, https://doi.org/10.1021/jo070607z.
[29] C. Wang, S. Cai, X. Li, X. Hu, J. Su, Z. Zhang, J. Han, Efficient organic dyes containing dibenzo heterocycles as conjugated linker part for dye-sensitized solar cells, Tetrahedron 69 (2013) 1970–1977, https://doi.org/10.1016/j.tet.2012.12.074.
[30] M. Klikar, I.V. Kityk, D. Kulwas, T. Mikysek, O. Pytela, F. Bureš, Multipodal arrangement of push-pull chromophores: a fundamental parameter affecting their electronic and optical properties, New J. Chem. 41 (2017) 1459–1472, https://doi.org/10.1039/c6nj02994a.
[31] M. Klikar, F. Bureš, O. Pytela, T. Mikysek, Z. Padělková, A. Barsella, K. Dorkenoo, S. Achelle, N., *N*′-Dibutylbarbituric acid as an acceptor moiety in push-pull chromophores, New J. Chem. 37 (2013) 4230–4240, https://doi.org/10.1039/c3nj00683b.
[32] M. Klikar, V. Jelínková, Z. Růžičková, T. Mikysek, O. Pytela, M. Ludwig, F. Bureš, Malonic acid derivatives on duty as electron-withdrawing units in push–pull molecules, Eur. J. Org. Chem. 2017 (2017) 2764–2779, https://doi.org/10.1002/ejoc.201700070.
[33] J. Korang, W.R. Grither, R.D. McCulla, Photodeoxygenation of dibenzothiophene S-oxide derivatives in aqueous media, J. Am. Chem. Soc. 132 (2010) 4466–4476, https://doi.org/10.1021/ja100147b.
[34] M. Blanchard-Desce, V. Alain, P.V. Bedworth, S.R. Marder, A. Fort, C. Runser, M. Barzoukas, S. Lebus, R. Wortmann, Large quadratic hyperpolarizabilities with donor-acceptor polyenes exhibiting optimum bond length alternation: correlation between structure and hyperpolarizability, Chem. Eur. J. 3 (1997) 1091–1104, https://doi.org/10.1002/chem.19970030717.
[35] D.B. Dess, J.C. Martin, Readily accessible 12-I-5 oxidant for the conversion of primary and secondary alcohols to aldehydes and ketones, J. Org. Chem. 48 (1983) 4155–4156, https://doi.org/10.1021/jo00170a070.
[36] F. Texier-Boullet, A. Foucaud, Knoevenagel condensation catalysed by aluminium oxide, Tetrahedron Lett. 23 (1982) 4927–4928, https://doi.org/10.1016/S0040-4039(00)85749-4.
[37] D. Cvejn, E. Michail, K. Seintis, M. Klikar, O. Pytela, T. Mikysek, N. Almonasy, M. Ludwig, V. Giannetas, M. Fakis, F. Bureš, Solvent and branching effect on the two-photon absorption properties of push-pull triphenylamine derivatives, RSC Adv. 6 (2016) 12819–12828, https://doi.org/10.1039/c5ra25170b.

[38] A. Isse, A.A., Gennaro, Absolute potential of the standard hydrogen electrode and the problem of interconversion of potentials in different solvents, J. Phys. Chem. B 114 (2010) 7894–7899.
[39] J.L. Sawyer, D.T. Sobkowiak, A. Roberts, Electrochemistry for Chemists, second ed., J. Wiley and Sons Inc., 1995, ISBN 978-0-471-59468-0.
[40] T. Kolev, I.V. Kityk, J. Ebothe, B. Sahraoui, Intrinsic hyperpolarizability of 3-dicyanomethylene-5,5-dimethyl-1-[2-(4-hydroxyphenyl)ethenyl]-cyclohexene nanocrystallites incorporated into the photopolymer matrices, Chem. Phys. Lett. 443 (2007) 309–312, https://doi.org/10.1016/j.cplett.2007.06.051.
[41] E. Cariati, C. Botta, S.G. Danelli, A. Forni, A. Giaretta, U. Giovanella, E. Lucenti, D. Marinotto, S. Righetto, R. Ugo, Solid state and solution fine tuning of the linear and nonlinear optical properties of (2-pyrene-1-yl-vinyl)pyridine by protonation-deprotonation reactions, Chem. Commun. 50 (2014) 14225–14228, https://doi.org/10.1039/c4cc05891g.
[42] K. Pielak, C. Tonnelé, L. Sanguinet, E. Cariati, S. Righetto, L. Muccioli, F. Castet, B. Champagne, Dynamical behavior and second harmonic generation responses in acido-triggered molecular switches, J. Phys. Chem. C 122 (2018) 26160–26168, https://doi.org/10.1021/acs.jpcc.8b08697.
[43] A. Majchrowski, I.V. Kityk, J. Ebothé, Influence of YAB: Cr3+ nanocrystallite sizes on two-photon absorption of YAB:Cr3+, Phys. Status Solidi Basic Res. 241 (2004) 3047–3055, https://doi.org/10.1002/pssb.200402071.
[44] Y. Qian, M. Cai, S. Wang, Y. Yi, Z. Shuai, G. Yang, Synthesis and third-order optical nonlinearities of nickel complexes of 8-hydroxyquinoline derivatives, Opt. Commun. 283 (2010) 2228–2233, https://doi.org/10.1016/j.optcom.2010.01.026.
[45] K. Ozga, A. Wojciechowski, M. Nabialek, M. Szota, M. Dospial, V. Kapustianyk, V. Rudyk, A.O. Fedorchuk, Specific features of photoinduced absorption and second harmonic generation of ferroic organic nanocomposites [C3H7NH3] 2MnCl4, Opt. Quant. Electron. 47 (2015) 743–753, https://doi.org/10.1007/s11082-014-9949-4.
[46] P. Szlachcic, A.A. Fedorchuk, A. Danel, B. Jarosz, A.M. El Naggar, A.A. Albassam, A. Wojciechowski, E. Gondek, T. Uchacz, K. Stadnicka, G. Lakshminarayana, I.V. Kityk, Optically operated second order optical effects in some substituted 4-(5-nitro-1,3-benzoxazol-2-yl)aniline chromophores, Dyes Pigments 141 (2017) 333–341, https://doi.org/10.1016/j.dyepig.2017.02.009.
[47] M.J. Frisch, G.W. Trucks, H.B. Schlegel, G.E. Scuseria, M.A. Robb, J.R. Cheeseman, G. Scalmani, V. Barone, G.A. Petersson, H. Nakatsuji, X. Li, M. Caricato, A.V. Marenich, J. Bloino, B.G. Janesko, R. Gomperts, B. Mennucci, H.P. Hratchian, J.V. Ortiz, A.F. Izmaylov, J.L. Sonnenberg, D. Williams-Young, F. Ding, F. Lipparini, F. Egidi, J. Goings, B. Peng, A. Petrone, T. Henderson, D. Ranasinghe, V.G. Zakrzewski, J. Gao, N. Rega, G. Zheng, W. Liang, M. Hada, M. Ehara, K. Toyota, R. Fukuda, J. Hasegawa, M. Ishida, T. Nakajima, Y. Honda, O. Kitao, H. Nakai, T. Vreven, K. Throssell, J.A. Montgomery Jr., J.E. Peralta, F. Ogliaro, M.J. Bearpark, J.J. Heyd, E.N. Brothers, K.N. Kudin, V.N. Staroverov, T.A. Keith, R. Kobayashi, J. Normand, K. Raghavachari, A.P. Rendell, J.C. Burant, S.S. Iyengar, J. Tomasi, M. Cossi, J.M. Millam, M. Klene, C. Adamo, R. Cammi, J.W. Ochterski, R.L. Martin, K. Morokuma, O. Farkas, J.B. Foresman, D.J. Fox, Gaussian 16, Revision A.03, 2016.
[48] O. Pytela, OPChem, http://bures.upce.cz/OPgm.
[49] O. Wennerstrom, V. Boekelheide, R.B. DuVernet, T. Otsubo, J. Lawson, Bridged [18]annulenes. A study of the synthesis and properties of 12c,12d,12e,12f-tetrahydrobenzo[g,h,i]perylene and its analogs, J. Am. Chem. Soc. 100 (1978) 2457–2464, https://doi.org/10.1021/ja00476a032.